

J3.4 USE OF AN ARTIFICIAL NEURAL NETWORK TO FORECAST THUNDERSTORM LOCATION: PERFORMANCE ENHANCEMENT ATTEMPTS

Waylon Collins* and Philippe Tissot**

*NOAA/National Weather Service

**Texas A&M University – Corpus Christi

1. INTRODUCTION

A feed-forward, supervised, multi-layer perceptron Artificial Neural Network (ANN) was developed to test the following hypothesis: An ANN can be developed to successfully forecast thunderstorm activity up to 24 hours in advance, and with a spatial accuracy of 20-km, wherein ANN inputs include selected output from (1) deterministic mesoscale Numerical Weather Prediction (NWP) models, and from (2) selected sub-grid scale data that contributes to convective initiation, or CI (Collins and Tissot, 2007, hereafter CT07.) We are not aware of any other project involving the use of both NWP output and sub-grid scale data, as inputs into an ANN, with the desire to forecast thunderstorm activity with an accuracy of 20-km. The underlying logic of this novel hypothesis is that the NWP model output provides a forecast of whether the larger mesoscale environment is conducive to CI while the sub-grid scale data determines the extent to which convection could be triggered at a particular location. The ANN serves as a means to map the highly non-linear relationship between the foregoing inputs and thunderstorm occurrence; an ANN model to forecast thunderstorms would result. This represents a paradigm shift away from the *sole* use of high-resolution (horizontal grid spacing ≤ 4 -km) NWP models to forecast thunderstorms, which, as suggested by Elmore et. al. (2002), may not be a reliable strategy. Results from CT07 were mixed: The model’s ability to forecast thunderstorm activity was encouraging, yet the number of false alarms was high. It was surmised that false alarms can be reduced by incorporating more relevant sub-grid scale data, and increasing the number of relevant NWP parameters that contribute to CI. This study represents such an attempt to improve the ANN’s performance. In Section 2, we discuss ANNs in a general sense. In Section 3, we describe the framework used to develop this ANN model. Section 4 contains a detailed description of the specific data inputs. In particular, we discuss how each parameter is related to thunderstorm development, and the specific data processing methods. In the final sections, the results (Section 5) and discussion and conclusions (Section 6) are presented. Portions of sections 2 and 4 contain information incorporated from our earlier study (CT07.)

2. ARTIFICIAL NEURAL NETWORKS

An Artificial Neural Network (ANN) is a computational model that attempts to account for the parallel nature of the human brain. Specifically, it is a network of highly interconnecting processing elements (neurons) operating in

- Corresponding author address: Waylon G. Collins, National Weather Service, 300 Pinson Drive, Corpus Christi, TX 78406; e-mail: Waylon.Collins@noaa.gov

parallel (Figure 1). An ANN can be used to solve problems involving complex relationships between variables. The particular type of ANN used in this study is a supervised one, wherein the observation (target) is specified, and the ANN is trained to minimize the error between the ANN output and the target, resulting in an optimal solution (assuming the global minimum is reached.) This is accomplished by adjusting the connections between the elements, which involves an adjustment to the weights ($w^1_{1,1} \dots w^1_{1,z}$ in figure 1.) In theory, this adjustment process can be viewed as a form of ‘learning’. Thus, the ANN is considered to be a form of artificial intelligence (AI). ANNs were selected for this study owing to their ability to model non-linear relationships. The relationship between the input and output parameters in this study is highly non-linear. Additional information on Artificial Neural Networks can be found in references such as Beale (1990) and Hagan et al. (1996).

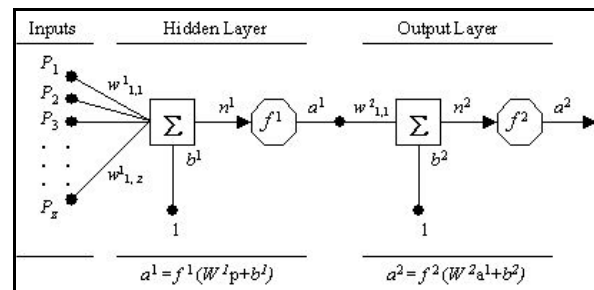


Figure 1: A 2-layer ANN with multiple inputs and single hidden and output neurons

3. ANN FRAMEWORK

3.1 ANN Domain

A grid of 13 x 22 equidistant points (20-km grid spacing) was developed which covers a region slightly larger than the County Warning and Forecast Area (CWFA) responsibility of the National Weather Service (NWS) forecasters in the Weather Forecast Office (WFO) in Corpus Christi Texas (CRP). These points create 286 square regions (hereafter referred to as ‘boxes’), each of which defines an area of 400 km² (figure 2). A 2-layer (one hidden layer, and one output layer), feed-forward, supervised ANN was utilized in this study. A framework was established (using MATLAB[®] software) to train 286 separate ANNs (one for each box region) to predict thunderstorm occurrence within each box. With respect to the forecasting of thunderstorms 3 to 24 hours in advance, NWS forecasters issue public forecasts on the probability of precipitation from thunderstorm activity. However, the highest forecast resolution for the NWS *Zone*

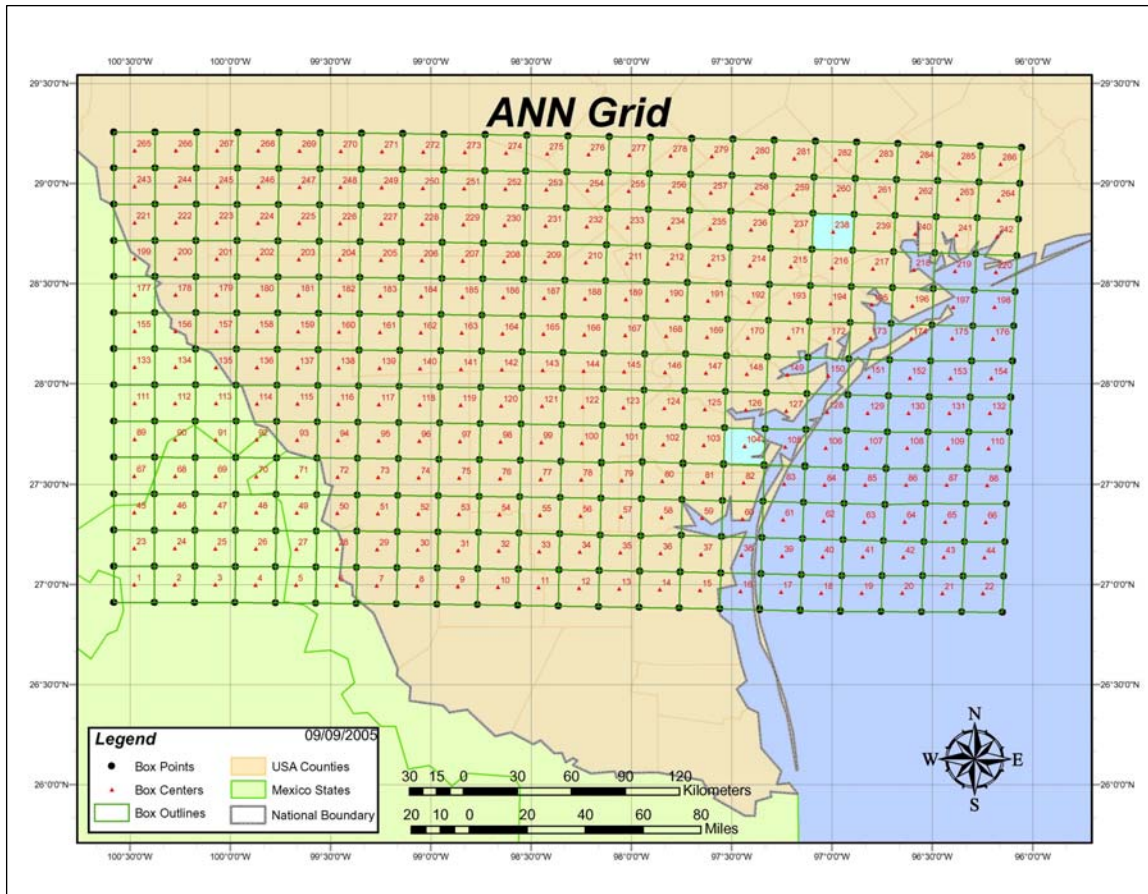


Figure 2: ANN Grid of 13 x 22 equidistant points. Northern (Southern) light blue box is labeled 238 (104).

Forecast is the county level. The median surface area of the 15 counties in the WFO CRP CWFA is approximately 2256 km². Thus an accuracy of 400 km² would be a significant improvement. For this study, only one box is examined – an inland region which includes Victoria, Texas (box 238 in figure 2).

3.2 ANN Target and Inputs

The model was developed based on data obtained from the period 1 June 2004 through 31 October 2007. Cloud-to-ground lightning data served as the proxy for thunderstorm activity and was also the target. The ANN input variables were chosen based on their physical relationship to thunderstorm development/dissipation. With respect to NWP model output, before 20 June 2006, the hydrostatic Eta was used as the NWP model. Afterward, the non-hydrostatic WRF-NMM (Janjic et al. 2001) was used. We introduce additional complexity by incorporating output from two unique NWP models. The Eta and WRF-NMM use different techniques to assimilate data, which will result in different initial conditions. Owing to the chaotic nature of the atmosphere, these initial condition differences can result in divergent deterministic solutions. Further, since one model is hydrostatic and the other non-hydrostatic, different solutions are likely. However, based on NWP model simulations, Weisman et al (1997) found that nonhydrostatic simulations effectively become hydrostatic with horizontal grid spacings > 8-km. Since the horizontal grid spacing of the WRF-NMM is 12-km, non-hydrostatic phenomena are not resolved (except

for mountain waves) which may decrease solution differences. Nevertheless, we assume that the model differences are not detrimental to this study.

Subgrid scale atmospheric processes that directly contribute to CI cannot be accounted for explicitly by the Eta or WRF-NMM. Thus, as mentioned previously, we incorporate such data. The subgrid scale parameters utilized in this study include proxies for soil moisture, wherein gradients of such contribute to local convergence which can trigger convection (e.g. Avissar and Liu, 1996). Further, the contribution of aerosols are included which can influence convective cloud dynamics (van den Heever, 2006).

3.3 ANN Forecast Strategy

In this study, we tested the ability of the ANN model to forecast CTG lightning occurrence in box 238 6 and 9 hours in advance. Figure 3 depicts the forecasting strategy. The inputs to the ANN (see section 4 for more details) are as follows:

- 1: NAM Forecasts of parameters 1-19 from the 1200 UTC cycle valid at 1800 UTC (2100 UTC.)
- 2: GOES AOD (parameter 39) observations at 1215, 1415, 1615, or 1815 UTC (Assumed equal to value at 1200 UTC).
- 3: NAM parameters 20-35 valid at 1200 UTC (output from model initialization)
- 4: Soil moisture-related variables (parameters 36-38) valid at 1200 UTC

The ANN output (thunderstorm forecast) is a value in the range [0..1], valid for 1800 UTC (2100 UTC.) The ANN was trained using cloud-to-ground lightning binary output as the target [0=no lightning; 1=lightning] Lightning “occurs” when at least 1 cloud-to-ground lightning strike occurs in box 238.

	1200 UTC (fcst hour=0)	1800 UTC (fcst hour=6)	2100 UTC (fcst hour=9)
ANN INPUTS	1. NAM parameters 20-35 2. Soil moisture proxies (parameters 36-38) 3. GOES AOD (parameter 39)	6-hour forecast of NAM parameters 1-19	9-hour forecast of NAM parameters 1-19
ANN OUTPUT		Thunderstorm prediction [0..1]	Thunderstorm prediction [0..1]
TARGET		Cloud-to-ground lightning binary output [0,1]	Cloud-to-ground lightning binary output [0,1]
AOD observations at 1215, 1415, 1615, or 1815 UTC; assumed equal to value at 1200 UTC Parameter 37 (Ndry) valid for previous day Parameters 36 (API gradients) and 38 (MPE gradients) valid for the antecedent 10-day period			

Figure 3: Thunderstorm ANN Forecast Strategy

3.4 ANN Training and Testing

The ANN model for this study was developed, trained, validated, and tested within the MATLAB[®] computational environment utilizing the Neural Network Toolbox (The MathWorks, Inc., 2006). The data set (1 June 2004 – 31 October 2007) was divided into a training set (40%), a validation set (20%), and a testing set (40%). All ANN models were trained using the automated regularization algorithm (trainbr) to improve generalization. The validation set served as a constraint on training, in order to minimize overfitting. The testing set was utilized to evaluate performance. The ANN architecture for this study is a feed-forward, supervised, multilayer perceptron (MLP) network with two (2) layers – one hidden layer and an output layer. Only one output neuron was used. The transfer function used in both the hidden and output layers (f^1 and f^2 in figure 1) is log-sigmoid. One hidden neuron was used for this study. MATLAB requires that the ANN model contain a full input set. Thus, cases missing an input or target value were eliminated. In the following section, we provide a detailed description of the target (a^2 in figure 1) and inputs (P_1, P_2, \dots, P_z in figure 1) to the ANN.

4. ANN TARGET AND INPUTS

4.1 Target Data (a^2)

Cloud to ground (CTG) lightning data (written to netCDF-formatted files) was obtained from the National Lightning Detection Network (NLDN) (e.g. Orville 1991). Computer scripts were used to extract hourly lightning data for each of the 286 boxes, and to write the output to a series of text files. The MATLAB[®] software was used to input the files then output the data into a target matrix. This data was used as a proxy for thunderstorm activity. Thus only thunderstorms that

generate CTG lightning strikes detected by NLDN are included. The target is binary (lightning versus no-lightning.)

Figure 4 reveals a 3-D display of the total number of CTG lightning strikes on the 13 x 22 ANN grid. Note that the greater number of lightning strikes occurred over the northeast region. This explains one reason for choosing northeast region box 238 – to provide the maximum amount of target data to train this supervised ANN.

4.2 Input Data (P_1, P_2, \dots, P_z)

4.2.1 NWP model output

The **first category** consists of thirty-five (35) output parameters from a hydrostatic mesoscale NWP model known as the Eta (e.g. Rogers et. al. 1996) [1 June 2004 – 19 June 2006] and a nonhydrostatic NWP model referred to as WRF-NMM (Janjic et. al. 2001) [20 June 2006 – 31 October 2007]. NCEP introduced the nomenclature NAM (North American Mesoscale), which does not refer to a model. Rather, the term NAM is simply a placeholder for the current operational mesoscale model running on a North American domain. Thus, before 19 June 2006, the NAM was the placeholder for the Eta model, and now is the placeholder for the WRF-NMM. Nevertheless, we will hereafter refer to WRF-NMM and Eta collectively as the NAM.

We utilized NAM output written to AWIPS (Advanced Weather Interactive Processing System) Grid 215 (Dey, 1998), a Lambert Conformal grid, with a horizontal grid spacing of 12-km (meso- γ scale.) Software written by Arthur Taylor (<http://www.weather.govmdl/degrib/>) of NOAA was used to extract the interpolated value of each parameter at the center of each box, which is assumed to be representative of the box. The output was written to a series of text files. Then, a MATLAB[®] software script was written to input these files to create a matrix containing the data.

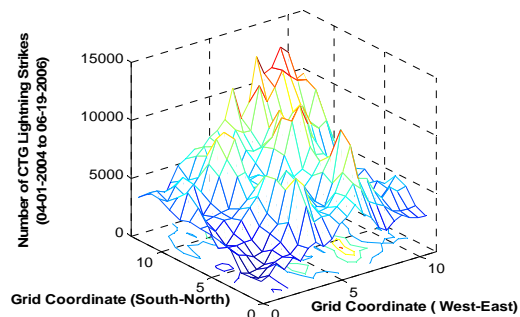


Figure 4: Total CTG Lightning Strikes (6-1-2004 to 6-19-2006) on the ANN grid. Point (0:0) represents the southwest corner (box 1)

CI requires sufficient **moisture** (to generate necessary hydrometeors), atmospheric **instability** (to generate updrafts strong enough to create a charge separation between the liquid and ice phases of water sufficient to generate lightning), and a **lifting mechanism** (to lift air parcels to the *level of free convection* (LFC), above which an unstable equilibrium exists). The NAM output parameters were chosen based on their contribution to the foregoing. As mentioned before, a

NWP model with a 12-km horizontal grid spacing is insufficient to explicitly forecast convection. However, the purpose of the numerical output is to provide a prediction of those parameters that contribute to CI/convective dissipation in the larger mesoscale environment (the subgrid scale processes that contribute to CI are accounted for in the parameters to be discussed later.) The following are the parameters and associated justifications.

Parameter 1: *Convective precipitation (CP)*

This is the precipitation that represents a byproduct of the CP process. This input is used because an objective of this study is to provide an ANN that will forecast the timing and positioning of convection more accurately than the NWP model. Ideally, the ANN will *learn* to correct CP scheme biases and generate more accurate forecasts.

Parameters 2-4: *Vertical Velocities at pressure levels 925, 700, and 500 millibars (VV925, VV700, VV500)*

In hydrostatic models (e.g. Eta), the vertical velocity term is diagnosed from predicted horizontal motions, instead of being predicted explicitly in non-hydrostatic models (e.g. WRF-NMM). VV925 and VV700 are used as proxies for lower level convergence (due to mesoscale phenomena such as sea breezes, and synoptic scale features including fronts) based on the reasoning that the continuity of mass relationship requires upward vertical velocities resulting from surface convergence. Surface convergence contributes to CI (e.g. Ulanski and Garstang 1978). However, due to its 12-km grid spacing, the Eta cannot resolve the storm scale divergence responsible for the initiation of individual convective cells. The purpose of VV700 and VV500 is to account for upper level disturbances. Operational experience at the NWS National Centers for Environmental Prediction (NCEP) Storm Prediction Center suggests that as many as 50% of thunderstorms are of the elevated variety (Banacos and Schultz, 2005). In these instances, the triggering mechanism is not a surface convergent feature (e.g. surface frontal boundary) but rather mid-level (between 900 and 600 mb) convergence (Wilson and Roberts 2006). The subsequent vertical motions would likely be captured at least by VV500. The unstable equilibrium aloft would be captured by the Lifted Index (LI), which will be discussed later.

Parameters 5-8: *U and V components of the wind at 10-m and 850 mb (u-10, v-10, u-850, v-850)*

Land surface heterogeneity contributes to micro-scale/meso- γ scale wind patterns that can trigger convection. However, strong wind can minimize the gradients generated by land surface heterogeneity (Dalu et al. 1996; Wang et al. 1996). The lead author postulates that strong wind will thus preclude thunderstorms that would otherwise be triggered by mesoscale gradients. Thus, it is important to include such wind as input to the ANN model. Further, the lead author has experienced a positive correlation between south/southwest wind at the 850 mb level and atmospheric stability sufficient to preclude CI over deep South Texas. It is hypothesized that such a stable equilibrium condition is caused by the advection of a drier and warmer mid level air mass moving across the region from Mexico.

Parameter 9: *Vertical wind shear between the surface (10-m) and 800 mb (sh0-8)*

Thunderstorm development within a particular 400 km² region can be influenced by phenomena in adjacent boxes. However, the ANN in this study does not explicitly account for such. The present ANN model predicts convection for a particular box solely based on information for that box. Including the sh0-8 prediction is one way to account for the influence of conditions over a broader spatial area. Rotunno et. al (1988) suggest that when a gust front (the leading edge of negatively-buoyant air generated by thunderstorms) moves into an environment with a certain shear profile in the lowest 2-km, the subsequent updraft is maximized, which can trigger additional convection. The sh0-8 parameter approximates the 0-2km vertical wind shear. Inputs to the ANN do not include specific information about the gust front. Thus, this parameter is only useful for cases wherein convection within a particular box is generated by gust fronts that enter the box from outside.

Parameter 10: *Vertical wind shear between 800mb and 600 mb (sh8-6)*

Crook (1996) has shown that convection initiation could be prevented by strong vertical wind shear above the planetary boundary layer. Vertical wind shear can preclude thunderstorm development if the updraft is weak (Colquhoun 1987). The sh8-6 parameter is used as a proxy for the vertical shear encountered by a parcel moving just above the boundary layer.

Parameters 11-14: *Precipitable water (PW), 850 mb mixing ratio, 850 mb relative humidity, and 2-m temperature*

Thunderstorms cannot develop without sufficient atmospheric moisture. PW is a proxy for atmospheric moisture by representing rainfall measurement that would occur if 100% of atmospheric moisture were to rain out. Yet, studies have shown the low level mixing ratio and relative humidity (RH) values have predictive value. Véronique, et al. (1998) found that the combination of CAPE (mentioned below), and RH in the lower levels, can help identify regions where convection is possible, synoptic weather pattern notwithstanding. Khairoutdinov and Randall (2006) found that high CAPE and low CIN are not quite sufficient for convective development. Rather, the horizontal scale of convective clouds must reach a threshold sufficient to overcome the dissipative effects of dry air entrainment, and that clouds tend to grow from air with the greatest water vapor content. Hence, we include the 850mb mixing ratio. The surface temperature was included since the maximum amount of moisture the air can hold is constrained by temperature.

Parameter 15: *Lifted Index (LI)*

The Lifted Index (LI) is simply the temperature difference between the environment and an ascending air parcel at the 500mb pressure level. A negative value indicates a parcel warmer than the surrounding environment, thus positively buoyant (unstable equilibrium). As such, it is a measure of atmospheric stability. Haklander and Delden (2003) found predictive value in the use of LI to forecast thunderstorms. Another purpose for inclusion of LI is to account for elevated

convection. Elevated convection tends to occur when upper level disturbances move across unstable equilibrium environments aloft. As mentioned before, VV700 and VV550 will serve as proxies for upper level disturbances, and the LI serves as a measure of upper level instability.

Parameters 16-17: *Convective Available Potential Energy (CAPE) and Convective Inhibition (CIN)*

CAPE measures the total energy available to generate thunderstorms. It is computed as the positive area on a thermodynamic diagram (e.g. SkewT-LogP). The greater this value, the greater the energy available for thunderstorm generation. Further, parcel theory indicates that the maximum speed of an updraft is a simple function of CAPE. However, updrafts in nature are generally weaker than what parcel theory suggests owing to aerodynamic drag, entrainment, compensating downward motions, and the weight of condensed water (e.g. Rogers and Yau, 1989.) The CIN measures the negative area on a thermodynamic chart, which typically represents an atmospheric layer with base at the surface. For non-elevated convection to occur, air parcels must be forced from the surface to the top of the CIN layer. However, if CIN is too strong, the parcel cannot reach the LFC and thus CI will not occur.

Parameter 18: *Potential Temperature Drop-off*

Crook (1996) has shown that convection tends to occur over areas wherein the potential temperature (temperature achieved when an air parcel is brought dry adiabatically to 1000 mb) in the boundary layer is lower than the value at the surface. Crook defined this difference as the potential temperature drop-off. However in this study, the proxy for the boundary layer potential temperature is the potential temperature at 900 mb.

Parameter 19: *Lifting Condensation Level (LCL)*

Although CAPE measures the total energy available for the conversion to upward vertical velocities, cloud base height (CBH) – according to Williams et. al (2005) – measures the efficiency of this process. A high CBH condition tends to be correlated with an environment that is more efficient than low CBH environments in the conversion to strong updrafts sufficient for thunderstorm development. The LCL is used as a proxy for CH.

Parameters 20-33: *U and V components of the wind at the surface, 900mb, 800mb, 700mb, 600mb, and 500mb at 12 UTC*

This data depicts wind velocity behavior at both the lower (sfc-700mb) and mid levels (700-500mb). The veering (backing) of geostrophic wind with height suggests warm (cold) air advection (e.g. Wallace and Hobbs 1977.) Although the wind is not geostrophic below 500 mb, it's assumed that the ageostrophic component of the wind does not prevent a positive correlation between veering or backing geostrophic and non-geostrophic wind. Hence, warm air advection (WAA) in the lower levels, in response to veering wind, will likely provide additional positive buoyancy to parcels below the LFC, with backing wind providing negative buoyancy. Yet, the opposite effects occur in the 700-500mb layer: WAA will likely provide negative buoyancy, while CAA in this layer will contribute to positive buoyancy. Thus, veering winds in the lower levels, or backing winds in the mid levels, will contribute to increased instability (or decreasing stability) and a greater chance for convection.

Results from a study by Findell and Eltahir (2003) added credence to this reasoning. The ANN should capture the foregoing relationship, hence the inclusion of this data as ANN inputs.

Parameters 34-35: *Low level humidity index and “Convective Triggering Potential”*

Findell and Eltahir (2003) developed a framework to assess the atmospheric controls on the interaction between soil moisture and the boundary layer. In particular, they found (among other things) that the 1200 UTC lower level (900-700mb) moisture and environmental lapse rates serve as constraints on afternoon convective development. They defined the humidity index (HI_{low}) as the sum of the dew point depressions at 950 and 850mb. They further defined a Convective Triggering Potential (CTP) as the area (on a thermodynamic diagram) between the moist adiabatic and the environmental temperature, in the 900-700mb layer. Essentially, the CTP measures the ambient environment's departure from the moist adiabatic rate in the 900-700mb layer. For this study, we incorporate HI_{low} , yet compute the ratio of the mean environmental lapse rate in the 900-700mb layer to the average moist adiabatic rate (assumed to be 6.5C/km in every case) as a proxy for CTP.

4.2.2 Subgrid scale data

The **second category** of input data includes data not explicitly accounted for owing to the 12-km grid spacing of the NAM. We incorporate four (4) variables in this category. The first, is derived from high resolution (4-km grid spacing) rainfall output from the *multi-sensor precipitation estimator (MPE)* algorithm (e.g. Fulton et. al 1998). From this data, the antecedent precipitation index or API, a soil moisture proxy, was calculated. For each day in box 238, the maximum gradient of API (**parameter 36**) was calculated. A major contributor to land surface heterogeneity, soil moisture gradients contribute to differential surface heating and subsequent microscale/meso- γ scale convergent wind patterns which in turn contribute to CI (e.g. Avissar and Liu 1996). Taylor and Lebel (1998), hereafter TL98, found a positive correlation between daily convective rainfall gradients and the corresponding 2 and 10-day antecedent gradients, over semi-arid locations on convective scales < 20-km. In particular, a positive feedback can occur whereby post convective evaporation contributes to soil moisture gradients resulting in areas favored for enhancement of subsequent convection/rainfall. According to TL98, this feedback occurs over 2 days due to strong soil moisture gradients that develop in response to bare soil evaporation. The 10-day correlation is related to evaporation of deeper soil moisture, from accumulated rainfall; yet this correlation was strongest when no rainfall occurred over during the preceding 4 days ($N_{dry}=4$). Since soil moisture gradients also contribute to convective initiation (Avissar and Liu 1996; Emori 1998), we incorporate 10-day antecedent MPE gradients and N_{dry} parameters, as the second and third (**Parameters 37-38**) sub-grid scale inputs in the ANN. The calculation of parameters 36-38 are explained in the Appendix. The fourth subgrid scale data ingest is the Aerosol Optical Depth or AOD (**Parameter 39**), which, according to van Den Heever (2006), may influence cloud microphysics, and subsequent storm updraft. We argue that a stronger updraft, due to aerosols, could conceivably result in a

thunderstorm, that otherwise would exist only as a convective shower (no lightning), without aerosol influence. Further, in their study of cloud-to-ground lightning over Houston, Texas for the period 1989-2000, Steiger et. al (2002) postulated that increased aerosol concentration may enhance the density of cloud-to-ground lightning strikes.

The AOD data set contains a significant amount of missing data. Thus, for each day of the time frame analyzed, data from the 1215, 1415, 1615, or 1815 UTC were used to increase the likelihood of acquiring valid data. Further, we assume that AOD is invariant during the 1200-1815 UTC period. This approach is somewhat reasonable as Anderson et. al. (2003) have shown that AOD temporal variations at a given location are not significant for time scales ≤ 6 hours. Each day, the earliest valid datum of the four was used to predict CI (see figure 3).

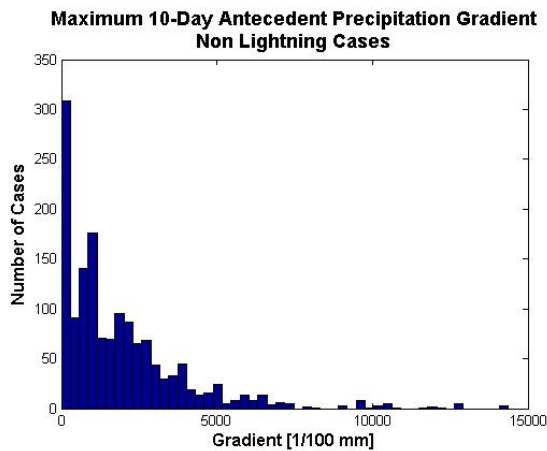


Figure 5a: Box 238 Histogram of maximum 10-day Antecedent Precipitation Gradient -- Non Lightning Cases (1-1-2003 to 10-31-2007). Gradient refers to finite differences. Units in 10^{-2} mm (5000×10^{-2} mm = 1.9685 in)

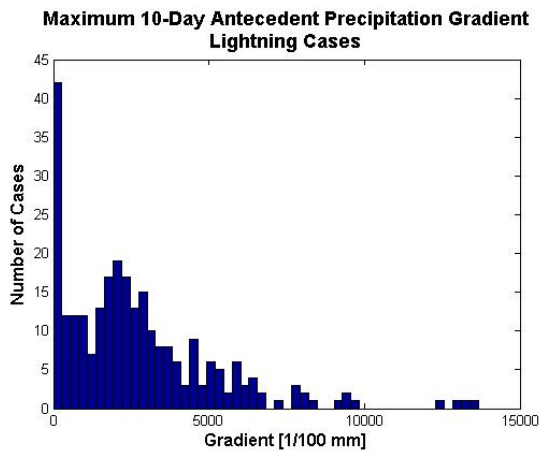


Figure 5b: Same as 5a, except for Lightning Cases.

Figure 5 depicts histograms of maximum 10-day antecedent MPE gradients, both for lightning and non-lightning cases, for the 1 January 2003 to 31 October 2007 period in box 238. Note that the highest frequency occurs at a larger gradient

magnitude for the lightning cases (ignoring zero frequency), consistent with the reasoning that a greater moisture gradient results in a greater chance for CI (assuming atmospheric conditions are favorable.)

Figure 6 depicts corresponding histograms of parameter N_{dry} . For each day in the data set, the number of dry days (no precipitation in box 238) for the previous 10 days was calculated. Then, the cases were segregated into lightning and non-lightning days for the creation of the histograms. Note that for the lightning cases, the frequency is highest for day 5. Yet for non-lightning cases, the frequency is highest for 8 of the 10-day antecedent period. These results suggest that more rain occurred during the 10-day period preceding lightning cases, along with a sufficient number of dry days to generate strong soil moisture gradients in response to the evaporation of deep soil moisture, consistent with TL98.

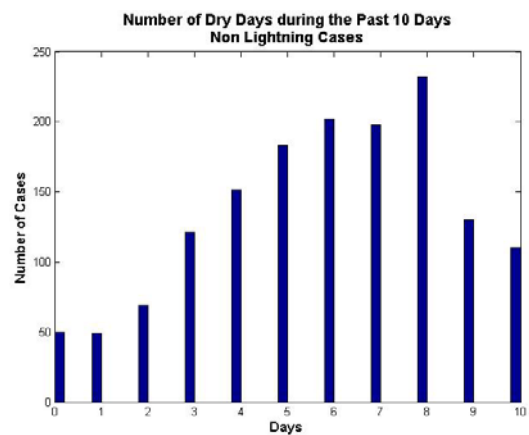


Figure 6a: Histogram of N_{dry} -- Non Lightning Cases (1-1-2003 to 10-31-2007).

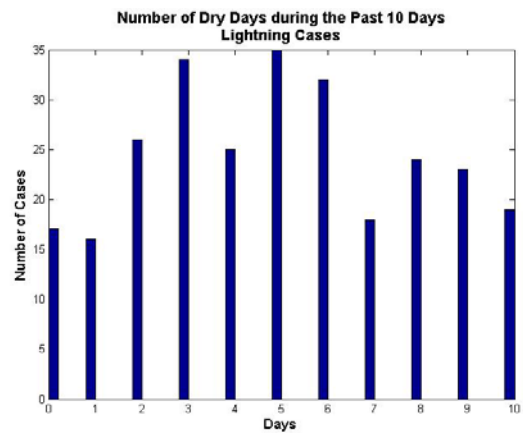


Figure 6b: Same as 6a, except for Lightning Cases

5. RESULTS

The utility of the ANN model in this study was evaluated using signal detection theory. In particular, we calculated the model's ROC (Relative Operating Characteristic) curves (Jolliffe and Stephenson, 2003). The ROC graphs the *probability of detection* (*POD*), and the *false alarm rate* (*FAR*). The ROC curve is

created by computing POD and FAR for varying ANN model thresholds, then graphing the POD as ordinate and FAR as abscissa. By thresholds, we refer to the minimum value of ANN output that is considered an ANN model prediction of the occurrence of a thunderstorm. We varied the threshold from 0.01 to 1.00 using a 0.01 increment. The results are depicted in figure 7. Figures 7a through 7d are based on 6-hour forecasts (F06) valid at 1800 UTC. An accurate forecast occurs when the model correctly predicts the target (for a given threshold) for the 4-hour window (W04) between 1600 and 2000 UTC. Figures 7e through 7h are based on 9-hour forecasts (F09) valid at 2100 UTC. An accurate forecast occurs when the model correctly predicts the target (for a given threshold) for the 4-hour (W04) window between 1900 and 2300 UTC. Note that skill has been demonstrated; the ROC curves for the testing sets are well above the diagonal for all thresholds. Thus, the ANN model developed in this study has demonstrated the ability to generalize.

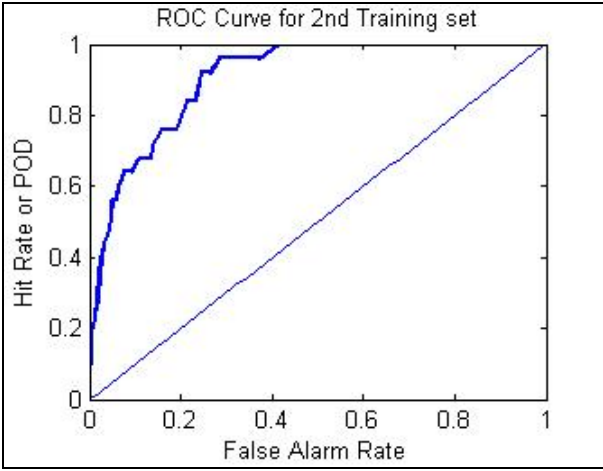


Figure 7c: ROC curve for 2nd training set: F06 W04

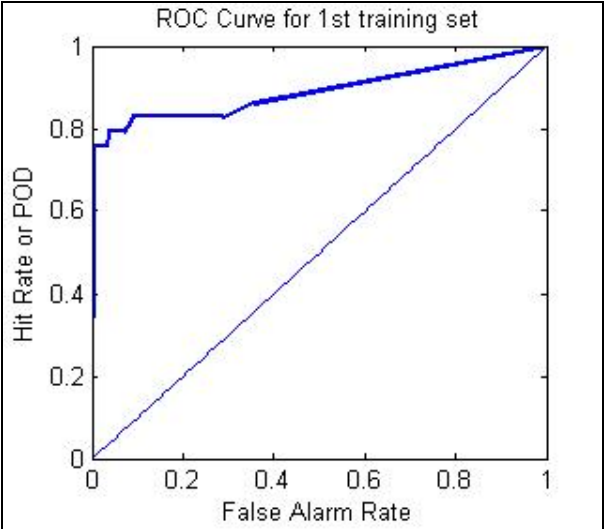


Figure 7a : ROC curve for 1st training set: F06 W04

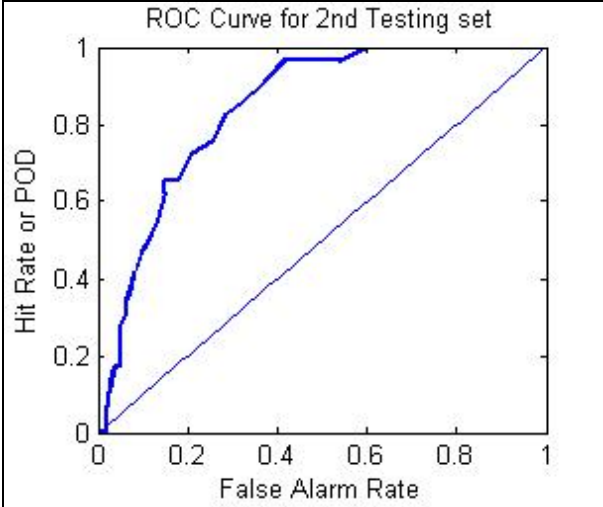


Figure 7d: ROC curve for 2nd testing set: F06 W04

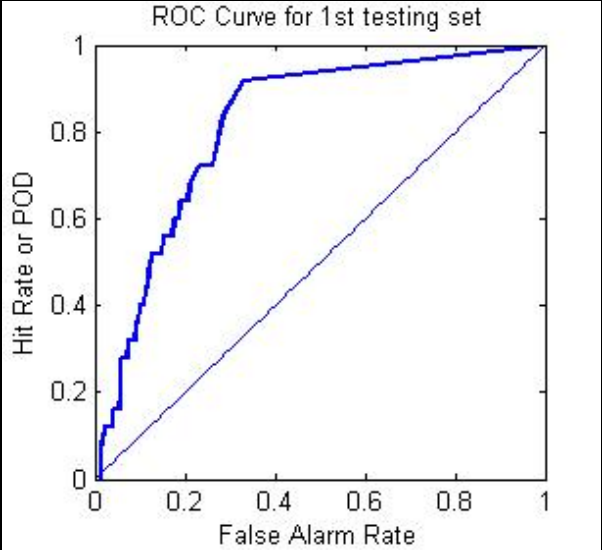


Figure 7b: ROC curve for 1st testing set: F06 W04

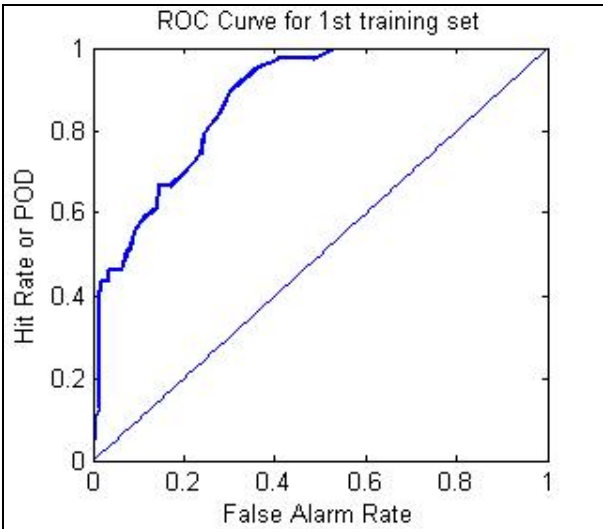


Figure 7e: ROC curve for 1st training set: F09 W04

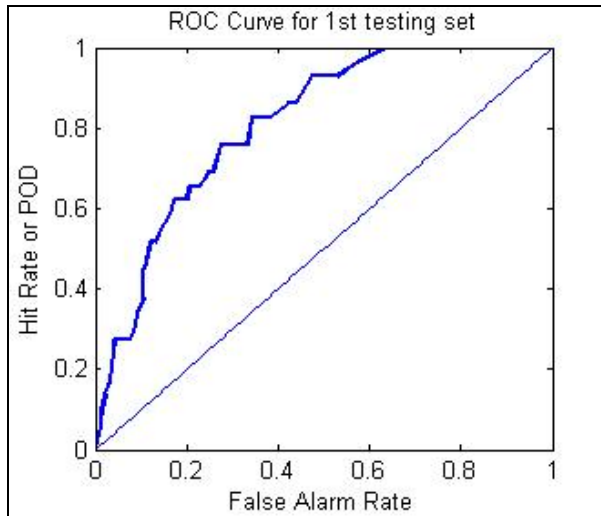


Figure 7f: ROC curve for 1st testing set: F09 W04

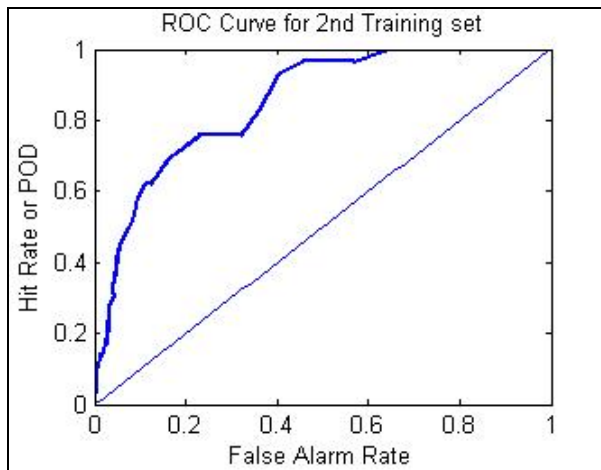


Figure 7g: ROC curve for 2nd training set: F09 W04

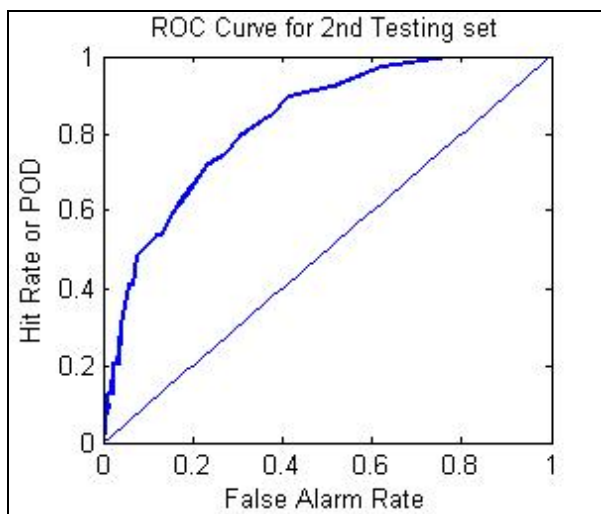


Figure 7h: ROC curve for 2nd testing set: F09 W04

6. DISCUSSION/CONCLUSIONS

We accessed the performance of an ANN modeling system, originally developed by CT07, after incorporating a more comprehensive set of inputs that contribute to CI. The 39 inputs include both NWP and sub-grid scale data, much of which possess a strong relationship to CI (not shown.) In this study, the ANN model was used to forecast the location of thunderstorms for 6 and 9 hours in advance, within a single 400 km² box region in South Texas. Evaluation of the ANN performance using ROC diagrams indicates that this ANN has the ability to generalize.

The implications of these results are significant. Instead of using a NWP model with high horizontal resolution (<4-km) to forecast thunderstorm location, one can develop an ANN model with the framework developed in this study – which includes a coarser resolution (e.g. 12-km) NWP model and sub-grid scale data – to generate thunderstorm forecasts, possibly with similar or greater accuracy and/or skill. This new modeling system will require significantly less computational expense for the NWP component.

Results notwithstanding, we seek to improve the accuracy of the model; we intend to focus on the following four areas for possible performance enhancement. First, we will test different ANN architectures, such as modular ANNs. Other connectionist architectures have performed better than MLPs. In other words, we want to determine whether an optimal solution can be achieved with ANN structures other than that of the MLP variety. Second, we will continue to search for additional sub-grid scale parameters. Thus, we assume that the highly nonlinear process of CI may not be fully accounted for in our ANN model. Data mining techniques may uncover additional physical parameters to incorporate. Third, we plan to address the fact that the atmosphere is chaotic. The use of ANN ensembles may provide a more accurate model. Fourth, we plan to compare the foregoing ROC curves to those generated based on WFO CRP forecaster output. This is important since the primary goal of this research is to develop an ANN model that can be used by the forecast community.

APPENDIX

Process of MPE Data Extraction

Estimates of rainfall were calculated by the NWS West Gulf River Forecast Center (WGRFC) using Stage III (Fulton et al. 1998) and Multi-sensor Precipitation Estimator (MPE) algorithms (hereafter MPE.) MPE estimates were on the 4-km Hydrological Rainfall Analysis Project (HRAP) Grid (polar stereographic projection) and written in a specialized format known as XMRG. Rick Hay, of the TAMUCC (Texas A&M University – Corpus Christi) Center of Water Supply Studies, wrote a Fortran program (nextextract) to extract MPE data for box 238 from XMRG files, and to write output to ASCII text, geocoded, time series files. MATLAB[®] code written by co-author Dr. Philippe Tissot to input MPE values from ASCII files and write to a 6 x 7 matrix (42 data points in box 238.)

API Calculation

For this study, the API was calculated based on the following equation from Cheng and Cotton (2004):

$API_t = MPE_t + \Pi(API)_{t-1}$ where t and t-1 refer to current and previous day, respectively. MPE is the sum of the 24 hourly MPE rainfall values for the current day. Π is the depletion coefficient:

$\Pi = 1 - 0.04\{\sin[2\pi((j-a-b)/c)] + 1\}$, where j=time in julian days, a=15 days, b=91.25, and c=365 days

Calculation of Parameter 36: Maximum API gradient

For each day in box 238, the API was calculated at each grid point [Owing to the 4-km grid spacing of the MPE data, and a 20-km x 20-km box region, 42 data points exist within each box]. Next, simple finite differences of API were calculated as the proxy for gradients. The maximum finite difference served as parameter 36.

Calculation of Parameter 37: 10-day antecedent maximum MPE gradient

For each day in box 238, the sum of hourly MPE rainfall values for the 10-day period, ending the previous day, was calculated at each grid point. Next, the maximum finite difference was determined, which served as parameter 37.

Calculation of Parameter 38: Number of dry days during the past 10 days (Ndry)

For each day in box 238, the number of days with no rainfall (based on MPE) during the 10-day period ending the previous day, was calculated. This served as parameter 38.

Acknowledgments. A number of individuals and organizations provided invaluable assistance. The Federal Aviation Administration (FAA) provided software that the lead author used to calculate the location of the gridpoints that describe the ANN grid. Former TAMUCC student Rick Smith utilized GIS software to confirm that the latitude/longitude values for the ANN domain were calculated correctly. Rick Hay provided software that allows for the extraction of MPE source data for each box region. Arthur Taylor (NOAA) provided software to extract the Eta output from Gridded Binary (GRIB) formatted files. Ingo Bethke provided software (<http://ferret.wrc.noaa.gov/Ferret>) to extract the target NLDN data from netCDF-formatted files. Irv Watson (WFO Tallahassee Florida) provided archived NLDN data for the June 2004-October 2005 period. Robert Rozumalski (NOAA) provided Eta output for the January-October 2005 period. Dan Swank (NCDC/NOMADS) provided the Eta output for the June-December 2004 period. Chuanyu Xu and Shobha Kondragunta (NOAA/NESDIS) provided GOES AOD data. The lead author received a 2005 U.S. Department of Commerce Pioneer Grant to purchase the necessary computer hardware, and the MATLAB[®] software, for this project. Niall Durham modified a PERL script which drastically decreased the computing time to process the NAM data. With respect to the generation of this manuscript, Natalia Nolzco provided excellent formatting and graphical assistance.

References

Anderson, T. L., R. J. Charlson, D. M. Winker, J. A. Ogren, K. Holmén, 2003: Mesoscale Variations of Tropospheric Aerosols. *J. Atmos. Sci.* **60**, 119-136.

Avissar, R., and Y. Liu. 1996. Three-dimensional numerical study of shallow convective clouds and precipitation induced by land surface forcing. *J. Geophys. Res.* **101**, 7499-7518.

Banacos, P. C., and D. M. Schultz. 2005. The Use of Moisture Flux Convergence in Forecasting Convective Initiation: Historical and Operational Perspectives. *Wea. Forecasting*, **20**, 351-366.

Beale, R. 1990. *Neural Computing: An Introduction*. Institute of Physics Publishing, London.

Collins, W. G., and P. Tisot, 2007: Use of an Artificial Neural Network to Forecast Thunderstorm Location, 5th Conference in the Application of Artificial Intelligence to Environmental Science, San Antonio, Texas, Amer. Meteor. Soc.

Colquhoun J. R., 1987: A Decision Tree Method of Forecasting Thunderstorms Serve a Thunderstorms and Tornadoes. *Wea. Forecasting*, **2**, 337-345.

Crook, N. A. 1996. Sensitivity of Moist Convection Forced by Boundary Layer Processes to Low-Level Thermodynamic Fields. *Mon. Wea. Rev.* **124**, 1767-1785.

Dalu, G. A., R. A. Pielke, M. Baldi, X. Zeng. 1996: Heat and Momentum Fluxes Induced by Thermal Inhomogeneities with and without Large-Scale Flow. *J. Atmos. Sci.* **53**, 3286-3302.

Dey, C. H., 1998: GRIB: The WMO Format for the Storage of Weather Product Information and the Exchange of Weather Product Messages in Gridded Binary Form as Used by NCEP Central Operations. *NWS Office Note 388*. NOAA/NWS, Washington, D.C.

Elmore, D. Stensrud, and K. Crawford, 2002: Explicit Cloud-Scale Models for Operational Forecasts: A Note of Caution. *Wea. Forecasting*, **17**, 873-884

Emori, S. 1998: The interaction of cumulus convection with soil moisture distribution: An idealized simulation. *Journal of Geophysical Research*, Vol. 103, No. D8, 8873-8884.

Fabry, F. 2006. The Spatial Variability of Moisture in the Boundary Layer and Its Effect on Convective Initiation: Project-Long Characterization. *Mon. Wea. Rev.* **134**, 79-91.

Findell, K. L., and E. A. B. Eltahir, 2003: Atmospheric controls on soil moisture-boundary layer interactions: Three-dimensional wind effects, *J. Geophys. Res.*, **108**(D8), 8383, doi:10.1029/2001JD001515, 2003.

Fulton, R. A., J. P. Breidenbach, D-J Seo, T. O'Bannon, and D. A. Miller, 1998: The WSR-88D Rainfall Algorithm. *Wea. Forecasting*, **13**, 377-395.

Hagan, M. T., H. B. Demuth, and M. Beale, 1996: *Neural Network Design*, International Thomson Publishing Inc.

Haklander, A. J., and A. Van Delden, 2003: Thunderstorm predictors and their forecast skill for the Netherlands. *Atmospheric Research*, **67-68**, 273-299.

- Janjic ZI, Gerrity JP, Nickovic S (2001) An Alternative Approach to Nonhydrostatic Modeling. *Monthly Weather Review*: Vol. **129**, No. 5 pp. 1164–1178
- Jolliffe I. T., and D. B. Stephenson, 2003: Forecast Verification: A Practitioner's Guide in Atmospheric Science. John Wiley & Sons Ltd, West Sussex, England. pp. 240.
- Khairoutdinov M., and D. Randall, 2006: High-resolution simulation of shallow-to-Deep Convection Transition over Land. *J. Atmos. Sci.* **63**, 3421-3436.
- Orville, R. E., 1991: Lightning ground flash density in the contiguous United States—1989. *Mon. Wea. Rev.*, **119**, 573–577
- Rogers, E., T. L. Black, D. G. Deaven, and G. J. DiMego, 1996: Changes to the operational “early” Eta analysis/forecast system at the National Centers for Environmental Prediction. *Wea. Forecasting*, **11**, 391–413.
- Rogers, R. R., and M. K. Yau, 1989: A Short Course in Cloud Physics. 3rd Edition, Elsevier Science, Burlington, MA. 290 pp.
- Rotunno, R., J. B. Klemp, and M. L. Weisman. 1988. A Theory for Strong, Long-Lived Squall Lines. *J. Atmos. Sci.* **45**, 464-485.
- Sánchez, J. L., E. G. Ortega, and J. L. Marcos, 2001: Construction and assessment of a logistic regression model applied to short-term forecasting of thunderstorms in Leon (Spain). *Atmospheric Research*, **56**, 57-71.
- Steiger, S. M., R. E. Orville, and G. Huffines, 2002: Cloud-to-ground lightning characteristics over Houston, Texas: 1989-2000. *Journal of Geophysical Research*, **107**, No. D11, 10.1029/2001JD001142
- Taylor, C. M., and T. Lebel, 1998: Observational Evidence of Persistent Convective-Scale Rainfall Patterns. *Monthly Weather Review*, 1597-1607.
- Ulanski, S. L., and M. Garstang. 1978. The role of surface divergence and vorticity in the life cycle of convective rainfall. Part I. Observations and analysis. *J. Atmos. Sci.* **35**, 1047-1062.
- Van den Heever, S.C., G. G. Carrió, W. R. Cotton, P. J. DeMott, and A. J. Prenni 2006: Impacts of Nucleating Aerosol on Florida Storms. Part I: Mesoscale Simulations. *J. Atmos. Sci.* **63**, 1752-1775
- Véronique Ducrocq, 1998: Diagnostic tools using a mesoscale NWP model for the early warning of convection. *Meteorol. Appl.* **5**, 329-349.
- Wallace, J. M, and P. V. Hobbs, 1977: *Atmospheric Science: An Introductory Survey*. Academic Press, New York.
- Wang, J., R. L. Bras, and E. A. B. Eltahir. 1996. A Stochastic Linear Theory of Mesoscale Circulation Induced by Thermal Heterogeneity of the Land Surface. *J. Atmos. Sci.* **53**, 3349-3366.
- Weisman, L.M., Skamarock, W.C. and Klemp, J.B., 1997. The resolution dependence of explicitly modeled convective systems. *Monthly Weather Review* **125**, pp. 527–548.
- Williams, E. R., V. Mushtak, D. Rosenfeld, S. Goodman, and D. Boccippio. 2005. Thermodynamic conditions favorable to superlative thunderstorm updraft, mixed phase microphysics and lightning flash rate. *Atmos. Res.*, **76**, 288-306.
- Wilson, J. W., and R. D. Roberts. 2006. Summary of Convective Storm Initiation and Evolution during IHOP: Observational and Modeling Perspective. *Mon. Wea. Rev.*, **134**, 23-47.